Available online at www.eccomasproceedia.org
Eccomas Proceedia COMPDYN (2025) 79-90

ECCOMAS
Proceedia

COMPDYN 2025
10th ECCOMAS Thematic Conference on
Computational Methods in Structural Dynamics and Earthquake Engineering
M. Papadrakakis, M. Fragiadakis (eds.)
Rhodes Island, Greece, 15-18 June 2025

ERROR BOUNDS IN COMPUTATIONAL DYNAMICS OF ROLLING HALF-DISK PROBLEMS: A COMPARATIVE ANALYSIS OF INTEGRATION METHODS

Ester Sallicandro[1], Luca Damiani[2], and Roberto Serpieri[2]

[1]Department of Engineering, University of Sannio
Piazza Roma 21, 82100 Benevento, Italy
e-mail: e.sallicandro@studenti.unisannio.it

[2] Department of Architecture and Industrial Design, University of Campania "Luigi Vanvitelli"
Via S. Lorenzo 1, 81031 Aversa (CE), Italy
e-mail: {luca.damiani1, roberto.serpieri}@unicampania.it

Abstract. *Modelling and integration of the transient response of freestanding bowl- and pot-shaped rigid objects under dynamic excitations, like bowls and vases subjected to seismic and environmental actions, pose applied and pure research problems that hold considerable interest in the protection of museum collections and archeological findings.*

The half disk model with its smooth convex boundary exempt from flat edges at the bottom, though of a simple archetypal nature, deserves consideration for modelling more elaborate bowl-like objects since it allows to circumvent the nontrivial problem of addressing the singularity arising in dynamic balance equations at time instants associated with the impact of flat edges, typically present in vases, while remaining rooted on canonical principles of Lagrangian Mechanics and on ordinary empirical postulates for sliding, rolling and impacting bodies. Accordingly, insights can be gained from the rolling half disk on the response of free-standing objects without resorting to additional heuristic postulates like angular momentum conservation at time instants of impact of flat edges, as proposed by some authors.

To properly discern physical dissipation from numerical dissipation in computational analyses, however, a proper investigation of algorithmic damping ratios and computational accuracy becomes mandatory. This contribution investigates the numerical stability and accuracy of the integration schemes employed for the half disk model, bringing a first comparison, based upon spectral radii analysis, among collocation methods, and setting a base for a forthcoming comparison with methods belonging to the Newmark family and with other widely employed approaches like linear and higher order multistep methods.

Keywords: Computational Mechanics, Differential Equation Integration, Numerical Methods, Analytical Methods, Heritage Preservation

---

Peer-review under responsibility of the organizing committee of COMPDYN 2025.
doi: 10.7712/120125.12393.25305

1 INTRODUCTION

Understanding the behavior of freestanding objects undergoing sliding-rolling motions in response to dynamic excitations is relevant to various mechanical applications among which the protection of museum exhibits with historical and artistic significance [1], [2], [3].

The rigid half-disk model provides an archetypal geometric and mechanical model employable to interpret, understand and describe the behaviour of bowl-shaped artifacts. The specific advantage brought by the smooth convex boundary of the half disk, compared to other rectangular or polygonal models [6], is that, being exempt from flat regions at the bottom, it offers a remedy to the nontrivial problem of addressing the singularity arising in dynamic balance equations occurring across time instants associated with the impact of flat edges [3], [4]. Accordingly, remaining rooted on canonical principles of Lagrangian Mechanics and on ordinary empirical postulates for sliding, rolling and impacting bodies [5], insights can be gained from the rolling half disk on the response of freestanding objects, without invoking additional heuristic postulates like angular momentum conservation at time instants of impact of flat edges, which have also been invoked in some past research works [6], [7].

Numerical results from an implementation in Matlab [15] of an analytical scheme devised by the authors [3], [4], based upon a general midpoint collocation method, which integrate the nonlinear equations of a rolling half-disk subjected to impulsive and sinusoidal excitations transmitted by a moving base, could recently find further numerical confirmation, on an empirical numerical basis, of the experimental evidence [8, 9] that sliding and friction coefficients as well as finishing properties of contacting surfaces are critical for capturing the true physical dissipation and the quality of motion to be expected. This contribution briefly reports some further recent numerical and analytical advancements on the accuracy, error bounding and stability of several investigated collocation schemes, which permit to compare the perfomances of several options for time collocation and which set a base for a forthcoming comparison with methods belonging to the Newmark family and with other widely employed approaches like linear and higher order multistep methods [10, 13].

2 Equation of Motion

The problem at hand involves a rolling homogeneous half-disk of radius R and area A, placed on a rigid horizontal base undergoing a prescribed horizontal translation with velocity v_B. It is assumed that rolling with no sliding occurs between the disk and the base. As illustrated in Fig. 1, the change of configuration of the system is defined by the rolling angle θ, positive if counterclockwise, and the prescribed horizontal translation $x_B(t)$ of the base. Points C, G and H are the center, centroid and contacting point in the reference configuration (dashed), respectively. Primed notation is used for the configuration in which the base alone has translated horizontally while the star indicates points in the current configuration of the system. The horizontal displacement of the disk center is $x_{\mathrm{C}}(t)$. The rolling constraint corresponds to:

$$x_{\mathrm{C}}(t) = x_B(t) - \theta(t)R, \tag{1}$$

where R is the radius of the disk which is assumed to be constant irrespective of the rolling rotation range. From a physical perspective, this assumption implies that, while the mass is distributed only in the half disk, the model, differently from what one would expect for a real half disk object, behaves as if the half disk would be capped by a massless half circumference, so that toppling of the object is not adressed. As illustrated in Fig. 1, the initial contacting point H is at the midpoint of the half circumference of the disk boundary.

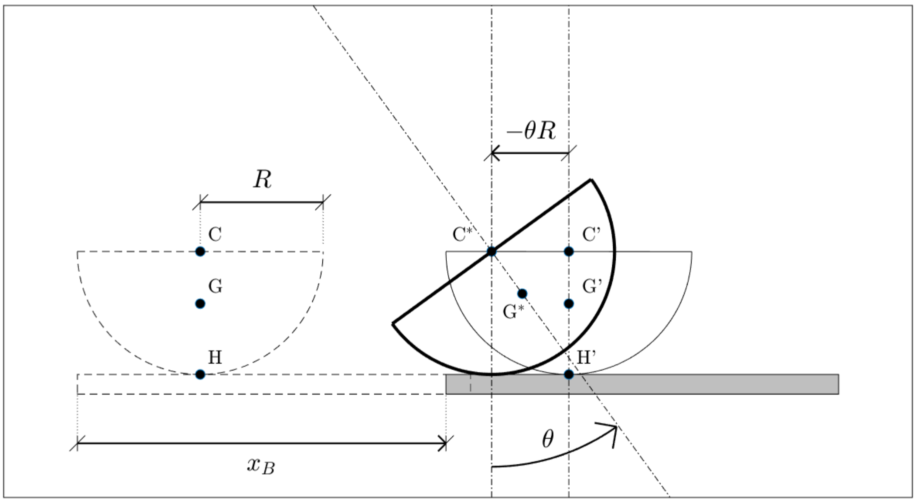

Figure 1: Kinematics of a rolling half disk on a sliding plane

Using a Lagrangian approach, the equation of motion for the idealized, non-dissipative, perfectly rolling model is derived from the Lagrange function $L(\theta,\dot{\theta})$ [3], [4], obtained as the difference by kinetic energy T and potential energy E_P:

$$T = \frac{1}{2} I_{\mathrm{G}} \dot{\theta}^2 + \frac{1}{2} A \left(R^2 + b^2 - 2Rb\cos\theta\right) \dot{\theta}^2 + A\left(2b\cos\theta - 2R\right) v_B \dot{\theta} + \frac{1}{2} A v_B^2, \tag{2}$$

$$E_P = \rho A g \left(R - b\cos\theta\right), \tag{3}$$

where I_{G} is polar moment of inertia of the disk about the center of mass, $b = \frac{4R}{3\pi}$ is the offset of the half disk's center from the centroid, ρ is the area density, and g is the gravitational acceleration. The resulting Lagrange function $L(\theta,\dot{\theta})$ is accordingly:

$$\begin{aligned} L(\theta,\dot{\theta}) \quad = \quad & \tfrac{1}{2} I_{\mathrm{G}} \dot{\theta}^2 + \tfrac{1}{2} A\left(R^2 + b^2 - 2Rb\cos\theta\right)\dot{\theta}^2 + \\ & A\left(2b\cos\theta - 2R\right) v_B \dot{\theta} + \tfrac{1}{2} A v_B^2 - \rho A g\left(R - b\cos\theta\right). \end{aligned} \tag{4}$$

From the least Action principle the following equation of motion is obtained from (4), which governs the dynamics of the rolling disk when no friction is considered:

$$\left[I_{\mathrm{G}} + A\left(R^2 + b^2\right)\right]\ddot{\theta} - 2ARb\cos\theta\ddot{\theta} + ARb\sin\theta\dot{\theta}^2 + Agb\sin\theta + A\left(-R + b\cos\theta\right)\dot{v}_B = 0. \tag{5}$$

Rolling friction is introduced by adding the dissipative term $c\dot{\theta}$ to (5), which represents a damping or braking moment:

$$\begin{aligned} & \left(I_{\mathrm{G}} + A\left(R^2 + b^2\right)\right)\ddot{\theta} - 2ARb\cos\theta\ddot{\theta} + ARb\sin\theta\dot{\theta}^2 + \\ & \qquad Agb\sin\theta + A\left(-R + b\cos\theta\right)\dot{v}_B + c\dot{\theta} \quad = \quad 0. \end{aligned} \tag{6}$$

A more compact equation of motion is achieved by the following positions:

$$\left(a_3 + a_4\cos\theta\right)\ddot{\theta} = a_1\sin\theta + a_2\sin\theta\dot{\theta}^2 + a_5\cos\theta\dot{v}_B + a_6\dot{v}_B + a_7\dot{\theta}, \tag{7}$$

where the constants $a_1, a_2, a_3, a_4, a_5, a_6, a_7$ are:

$$a_1 = -\frac{2}{3}\frac{g}{R}, \quad a_2 = -\frac{2}{3}, \quad a_3 = \frac{3}{4}\pi, \quad a_4 = -\frac{4}{3},$$
$$a_5 = -\frac{2}{3}R, \quad a_6 = \frac{1}{2}\frac{\pi}{R}, \quad a_7 = -\frac{c}{R^4}.$$

The equation of motion is finally given normal form by expressing it as the following non-linear system of two first-order differential equations

$$\begin{cases} \dot{\theta} = f_\theta(\theta, \omega) \\ \dot{\omega} = f_\omega(\theta, \omega) \end{cases} \tag{8}$$

where $f_\theta(\theta, \omega)$ and $f_\omega(\theta, \omega)$ are:

$$f_\theta(\theta, \omega) = \omega, \tag{9}$$
$$f_\omega(\theta, \omega) = \frac{a_1 \sin\theta + a_2 \sin\theta\omega^2 + a_5 \dot{v}_B \cos\theta + a_6 \dot{v}_B + a_7 \omega}{a_3 + a_4 \cos\theta}. \tag{10}$$

3 INTEGRATION SCHEME

The scheme employed for integrating (8) exploits a piecewise linear interpolation of θ and ω in time and midpoint collocation. The time interval $[t_0, t^*]$ is discretized into N equal time steps of size $h = t_{n+1} - t_n$, and the differential problem is converted into an algebraic system. The primary unknowns, θ_n and ω_n, are iteratively solved at each n-th time step.

For each n, the midpoint $t_m = (t_n + t_{n+1})/2$ of the generic time interval $[t_n, t_{n+1}]$ is computed and, based on linear interpolation, midpoint values of primary functions θ_m and ω_m are computed as well as their time derivatives $\dot{\theta}_m$ and $\dot{\omega}_m$.

By applying midpoint collocation to system (8), the differential equations are transformed into the following nonlinear algebraic system:

$$\begin{cases} \dot{\theta}_m = f_\theta(\theta_m, \omega_m) = \omega_m \\ \dot{\omega}_m = f_\omega(\theta_m, \omega_m) = \dfrac{a_1 \sin\theta_m + a_2 \sin\theta_m \omega_m^2 + a_7 \omega_m + a_5 \dot{v}_B \cos\theta_m + a_6 \dot{v}_B}{a_3 + a_4 \cos\theta_m}. \end{cases} \tag{11}$$

Substitution of the midpoint interpolated values for θ_m and ω_m into (11) leads to the following nonlinear algebraic system:

$$\begin{cases} \dfrac{\theta_{n+1}}{h} - \dfrac{\theta_n}{h} = F_\theta(\theta_{n+1}, \omega_{n+1}) \\ \dfrac{\omega_{n+1}}{h} - \dfrac{\omega_n}{h} = F_\omega(\theta_{n+1}, \omega_{n+1}) \end{cases} \tag{12}$$

which is expressed in terms of two functions F_θ and F_ω:

$$F_\theta(\theta_{n+1}, \omega_{n+1}) = f_\theta(\theta_m, \omega_m) = f_\theta\left(\frac{\theta_n + \theta_{n+1}}{2}, \frac{\omega_n + \omega_{n+1}}{2}\right), \tag{13}$$
$$F_\omega(\theta_{n+1}, \omega_{n+1}) = f_\omega(\theta_m, \omega_m) = f_\omega\left(\frac{\theta_n + \theta_{n+1}}{2}, \frac{\omega_n + \omega_{n+1}}{2}\right). \tag{14}$$

To solve system (12), a first-order linear approximation is applied to $F_\omega(\theta_{n+1}, \omega_{n+1})$ via a power series expansion:

$$F_\omega(\theta_{n+1}, \omega_{n+1}) \approx F_\omega(\theta_n, \omega_n) + \left.\frac{\partial F_\omega}{\partial \theta_{n+1}}\right|_{\theta_n, \omega_n} (\theta_{n+1} - \theta_n) + \left.\frac{\partial F_\omega}{\partial \omega_{n+1}}\right|_{\theta_n, \omega_n} (\omega_{n+1} - \omega_n), \quad (15)$$

whereby the following system is obtained:

$$\begin{aligned} \frac{\theta_{n+1}}{h} - \frac{\theta_n}{h} &= \frac{\omega_n}{2} + \frac{\omega_{n+1}}{2}, \\ \frac{\omega_{n+1}}{h} - \frac{\omega_n}{h} &= F_\omega(\theta_n, \omega_n) + \frac{\partial F_\omega}{\partial \theta_{n+1}}(\theta_{n+1} - \theta_n) + \frac{\partial F_\omega}{\partial \omega_{n+1}}(\omega_{n+1} - \omega_n). \end{aligned} \quad (16)$$

Upon rearranging terms of (16), the implicit iterative scheme is obtained:

$$\begin{bmatrix} 1 & -\frac{h}{2} \\ -\frac{h}{2}\frac{\partial F_\omega}{\partial \theta_{n+1}} & 1 - h\frac{\partial F_\omega}{\partial \omega_{n+1}} \end{bmatrix} \begin{bmatrix} \theta_{n+1} \\ \omega_{n+1} \end{bmatrix} = \begin{bmatrix} \theta_n + \frac{h}{2}\omega_n \\ hF_\omega(\theta_n, \omega_n) - h\frac{\partial F_\omega}{\partial \theta_{n+1}}\theta_n + (1 - h\frac{\partial F_\omega}{\partial \omega_{n+1}})\omega_n \end{bmatrix} \quad (17)$$

which can be solved to finally provide θ_{n+1} and ω_{n+1}:

$$\begin{bmatrix} \theta_{n+1} \\ \omega_{n+1} \end{bmatrix} = \frac{1}{\Delta} \begin{bmatrix} 1 - h\frac{\partial F_\omega}{\partial \omega_{n+1}} & \frac{h}{2} \\ \frac{h}{2}\frac{\partial F_\omega}{\partial \theta_{n+1}} & 1 \end{bmatrix} \begin{bmatrix} \theta_n + \frac{h}{2}\omega_n \\ hF_\omega(\theta_n, \omega_n) - h\frac{\partial F_\omega}{\partial \theta_{n+1}}\theta_n + (1 - h\frac{\partial F_\omega}{\partial \omega_{n+1}})\omega_n \end{bmatrix}, \quad (18)$$

with Δ being the determinant of the coefficient matrix on the left-hand side of (17):

$$\Delta = 1 - h\frac{\partial F_\omega}{\partial \omega_{n+1}} - \frac{h^2}{4}\frac{\partial F_\omega}{\partial \theta_{n+1}}. \quad (19)$$

All matrices in (18) are updated at each time step based on the values of the previous time instant and of the updated acceleration $\dot{v}_B$ of the supporting base. This iterative process provides, proceeding from the initial boundary conditions $[\theta_0, \omega_0]^T$, the discretized solution of system (7).

4 RESULTS

4.1 General model behavior

The general behaviour of the rolling disk under large base displacements, large rotations and nonzero friction, as provided by Eq. (7) and integrated by scheme (18), can be appreciated by comparing the time-history results of Figs. (2) and (3) corresponding to two examples which differ by the friction coefficient alone, being $c = 0.082$ and $c = 0.8$ m^4/s, respectively. Both examples concern a same half disk with $R = 0.5$ m subjected to a same sinusoidal base excitation of amplitude 0.30 m and frequency of 1.0 Hz prescribed for x_B. In both examples the integration covers a time lasting 20 s and employs 400 time steps. A necessary reminder for interpreting the results presented is that, as specified above, since Eqs. (1) and (7) do not account for curvature radius of the boundary different from R, the obtained mathematical solution for angles $\pi/2 + 2k\pi < \theta < -\pi/2 + 2(k+1)\pi$, with $k \in \mathbb{Z}$, describes the configuration of a half disk rolling over a half circular 'cap', with the half disk center C remaining at the same fixed height R, as in ordinary configurations with $-\pi/2 + 2k\pi < \theta < +\pi/2 + 2k\pi$.

Comparison of Figs 2 and 3 shows the critical sensitivity of the induced motion to variations in rolling friction. Specifically, the rolling coefficient c discriminates the long-term behavior of

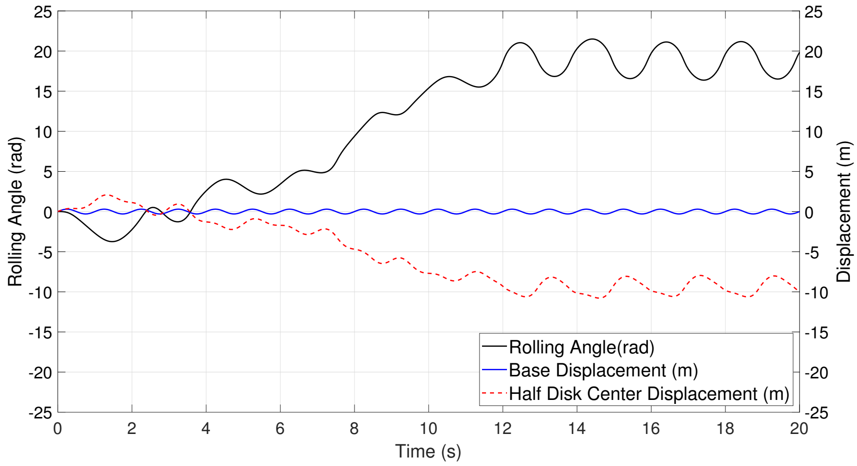

Figure 2: Rolling angle, half disk and base displacements, $c = 0.082$ m^4/s

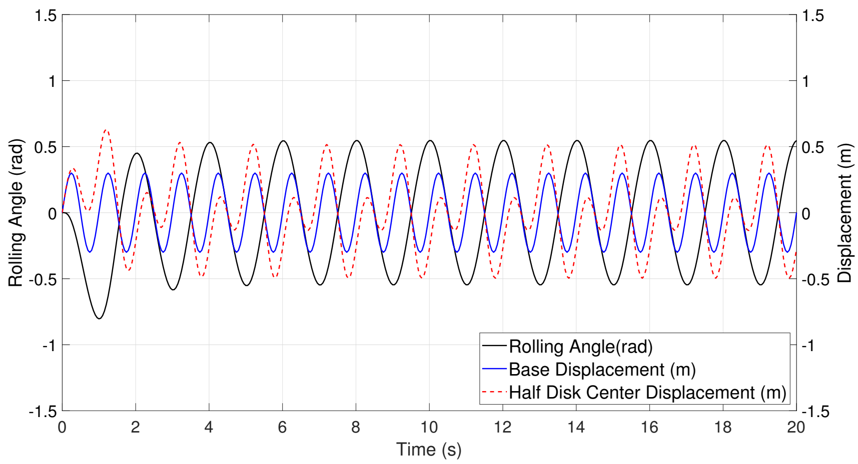

Figure 3: Rolling angle, half disk and base displacements, $c = 0.8$m^4/s

the system. Depending on its value, the motion can either settle into a new oscillatory equilibrium position or continue oscillating around the initial original position of the disk (relative to the moving base). When c is sufficiently low, the damping effect becomes more pronounced, leading to the stabilization of the oscillations around a new center of motion. Conversely, for higher values of c, the system retains its oscillatory behavior around its initial position.

4.2 Error bounds

In this opening study, the error bounds and the accuracy of the integration scheme presented in Sect. 3 are preventively examined over a simplified problem by confining the analyses of Sect. 4.1 to small rotations and to a fixed supporting base. A specific reference is also made to a model sized over the marble half cylinder shown in Fig. 4, having a radius of approximately 7 cm. Moreover, since, under a computational stability perspective, absence of damping is a more demanding condition [13], the integration scheme has been investigated assuming zero rolling friction.

Altogether, the above selected model testing hypotheses imply the specialization of Eq. (5) to:

$$\ddot{\theta} = -\frac{Agb}{I_{\mathrm{G}} + A(R-b)^2}\theta. \tag{20}$$

Figure 4: Marble cylindrical specimen, radius 7 cm

By introducing the natural frequency of the system, as recovered from the simplified model at hand,

$$\overline{\omega}_0^2 = -\frac{Agb}{I_{\mathrm{G}} + A(R-b)^2} = \frac{g}{R} \cdot \frac{2}{3} \cdot \frac{1}{\frac{3\pi}{4} - \frac{4}{3}}, \tag{21}$$

the mathematical form of the harmonic oscillator equation, can be emphasized:

$$\ddot{\theta} = -\overline{\omega}_0^2 \theta \tag{22}$$

and, after some elaborations not reported herein, Eqs. (18) and (19) achieve the form:

$$\begin{bmatrix} \theta_{n+1} \\ \omega_{n+1} \end{bmatrix} = \frac{1}{1 + \frac{\overline{\omega}_0^2 h^2}{4}} \begin{bmatrix} 1 - \frac{\overline{\omega}_0^2 h^2}{4} & h \\ -\overline{\omega}_0^2 h & 1 - \frac{\overline{\omega}_0^2 h^2}{4} \end{bmatrix} \begin{bmatrix} \theta_n \\ \omega_n \end{bmatrix}. \tag{23}$$

In the sequel, error bounds to scheme (23) are first developed and discussed in general terms, to be finally quantitatively appreciated for the small oscillations of the marble piece of 7 cm of radius.

The exact solution in normal form corresponding to time t_i, its corresponding algorithimic approximation, and the initial boundary conditions are respectively denoted as:

$$\boldsymbol{y}_i = \begin{bmatrix} \theta_i \\ \omega_i \end{bmatrix}, \qquad \tilde{\boldsymbol{y}}_i = \begin{bmatrix} \tilde{\theta}_i \\ \tilde{\omega}_i \end{bmatrix}, \qquad \boldsymbol{y}_0 = \begin{bmatrix} \theta_0 \\ \omega_0 \end{bmatrix}. \tag{24}$$

The error $e_i^{(k)}$ is defined as the Euclidean (not dimensionally homogeneous) norm of the difference between the approximate solution at time t_i, as obtained from scheme 23 after k consecutive iterations, and the exact solution relevant to the same time instant, $\boldsymbol{y}_i$:

$$\boldsymbol{\delta}_i^{(k)} = \tilde{\boldsymbol{y}}_i^{(k)} - \boldsymbol{y}_i, \qquad e_i^{(k)} = \left\| \boldsymbol{\delta}_i^{(k)} \right\|, \tag{25}$$

so that $\boldsymbol{\delta}_1^{(1)} = \tilde{\boldsymbol{y}}_1^{(1)} - \boldsymbol{y}_1$ is the corresponding vector difference after the first time step.

Since many works have compared several parametric updating options in search for optimal schemes [10, 13], the optimality of midpoint collocation has been also investigated for the half disk by defining the collocation point in the parametric form $t_c = t_n + \alpha_c h$ with $0 \leq \alpha_c \leq 1$.

Upon giving such parametric form to the present scheme, the following approximate small-displacement solution results for the first time step:

$$\tilde{\boldsymbol{y}}_1^{(1)} = \begin{bmatrix} 1 - \frac{q}{\alpha_c(1+q)} & \frac{h}{1+q} \\ -\frac{q}{\alpha_c^2 h(1+q)} & 1 - \frac{q}{\alpha_c(1+q)} \end{bmatrix} \boldsymbol{y}_0, \tag{26}$$

in which $q = (\overline{\omega}_0 h \alpha_c)^2$, and the matrix on the right is denoted as $\boldsymbol{A}$.
The exact solution to (22), customarily provided in the form of an infinite series by the method of undetermined coefficients, can be set in the same matrix arrangement of Eq. (26):

$$\boldsymbol{B} = \begin{bmatrix} \sum_{k=0}^{\infty} \frac{(-1)^k}{(2k)!} r^{2k} & \frac{1}{\overline{\omega}_0} \sum_{k=0}^{\infty} \frac{(-1)^k}{(2k+1)!} r^{2k+1} \\ -\overline{\omega}_0 \sum_{k=0}^{\infty} \frac{(-1)^k}{(2k+1)!} r^{2k+1} & \sum_{k=0}^{\infty} \frac{(-1)^k}{(2k)!} r^{2k} \end{bmatrix}, \quad \boldsymbol{y}_1 = \boldsymbol{B}\boldsymbol{y}_0. \tag{27}$$

The expressions in summation in the entries of matrix B in (27) are trivially recognized to be the basic trigonometric functions. By subtracting from (26) the second of (27) and using the more compact and traditional sine and cosine notations, the difference between the exact and the approximate numerical solution of scheme (26) for the single time step is obtained. Such difference provides the argument of the error norm whose bounds are herein investigated:

$$\tilde{\boldsymbol{y}}_1^{(1)} - \boldsymbol{y}_1 = \begin{bmatrix} 1 - \frac{q}{(1+q)\alpha_c} - \cos r & \frac{h}{(1+q)} - \frac{1}{\overline{\omega}_0} \sin r \\ -\frac{q}{\alpha_c^2 h(1+q)} + \overline{\omega}_0 \sin r & 1 - \frac{q}{(1+q)\alpha_c} - \cos r \end{bmatrix} \boldsymbol{y}_0. \tag{28}$$

This last matrix can be given the simpler form:

$$\boldsymbol{C} = \begin{bmatrix} c_{11} & c_{12} \\ -\overline{\omega}_0^2 c_{12} & c_{11} \end{bmatrix}, \tag{29}$$

and applying a power series expansion, the coefficients c_{11} and c_{12} of (29) are computed:

$$c_{11} = r^2 \left(-\alpha_c + \frac{1}{2} \right) - \frac{q}{\alpha_c} \sum_{k=1}^{\infty} (-q)^k - \sum_{k=1}^{\infty} \frac{(-1)^{k+1}}{[2(k+1)]!} r^{2(k+1)}, \tag{30}$$

$$c_{12} = h \sum_{k=0}^{\infty} (-q)^k - \frac{1}{\overline{\omega}_0} \sum_{k=0}^{\infty} (-1)^k \frac{1}{(2k+1)!} r^{2k+1}. \tag{31}$$

Since an objective of the method is to minimize c_{11} and c_{12} to minimize the error, an optimal choice for α_c is soon recognized to be $1/2$. Upon setting $\alpha_c = 1/2$ in (30), the residual term $\mathrm{RES}_{c_{11}}$ which builds the error of the method for c_{11} turns out to be:

$$\mathrm{RES}_{c_{11}} = \frac{q}{\alpha_c} \sum_{k=1}^{\infty} (-q)^k - \sum_{k=1}^{\infty} \frac{(-1)^{k+1}}{[2(k+1)]!} r^{2(k+1)}. \tag{32}$$

It can be shown that combination of the two sums in (32) is an alternating series whose individual terms converge to zero as $k \to \infty$, and that few more elaborations lead to the following representation:

$$\mathrm{RES}_{c_{11}} = \sum_{k=1}^{\infty} (-1)^{k+1}\, \alpha_c^{2(k+1)}\, r^{2(k+1)} \left\{ \frac{1}{\alpha_c} - \frac{1}{\alpha_c^{2(k+1)}[2(k+1)]!} \right\}. \tag{33}$$

Accordingly, series (33) satisfies the conditions of Leibniz's theorem, so that coefficient c_{11} has the following bound which is the first term of the series:

$$c_{11} \leq \frac{(\overline{\omega}_0 h)^4}{12}. \tag{34}$$

By a similar reasoning on (31) and recalling (29), it can be shown that c_{12} and c_{21} admit the following bounds:

$$|c_{12}| \leq \frac{\overline{\omega}_0^2 h^3}{12}, \qquad |c_{21}| \leq \frac{\overline{\omega}_0^4 h^3}{12}. \tag{35}$$

The bounds so far computed can be assembled into the following matrix

$$\boldsymbol{M_C} = \frac{\overline{\omega}_0^2 h^3}{12} \begin{bmatrix} \overline{\omega}_0^2 h & 1 \\ \overline{\omega}_0^2 & \overline{\omega}_0^2 h \end{bmatrix} \tag{36}$$

which, as it can be shown, is such that, for any arbitrary vector $\boldsymbol{u} \in \mathbb{R}^2$, $\|\boldsymbol{M_C u}\| \geq \|\boldsymbol{C u}\|$.

By iteratively combining (24)-(30) to express the total difference $\boldsymbol{\delta}_n^{(n)}$, after n steps, between transcendent solution and algorithmic solution, it can be also shown that (elaborations are omitted to contain the length of this communication):

$$\boldsymbol{\delta}_n^{(n)} = \left(\sum_{k=0}^{n-1} \boldsymbol{A}^{(n-k-1)} \boldsymbol{C} \boldsymbol{B}^k \right) \boldsymbol{y_0}. \tag{37}$$

The bounding problem amounts to finding a real number $M_n^{(n)}$, suitable for the application at hand, such that the inequality $e_n^{(n)} \leq M_n^{(n)} \|\boldsymbol{y_0}\|$ over the total error $e_n^{(n)} = \left\| \boldsymbol{\delta}_n^{(n)} \right\|$ holds for any vector of initial values $\boldsymbol{y_0}$, and to accordingly calibrate a suitable number of time steps.

A suitable bound has been obtained from elaboration of the spectral radii of the matrices $\boldsymbol{A}$, $\boldsymbol{M}_C$ and $\boldsymbol{B}$ based upon polar and spectral matrix decompositions. Since al three matrices are not symmetric, the largest eigenvalues in absolute value have been computed for matrices $\boldsymbol{A}$, $\boldsymbol{M}_C$ and $\boldsymbol{B}$ as well as for matrices $\boldsymbol{A}^T\boldsymbol{A}$, $\boldsymbol{M}_C^T\boldsymbol{M}_C$ and $\boldsymbol{B}^T\boldsymbol{B}$, resulting into complex moduli for the former three matrices and real moduli for the last three ones.

An upper bound associated with matrix $\boldsymbol{B}$, r_B, has been computed as the square root of the maximum eigenvalues of matrix $\boldsymbol{B}^T\boldsymbol{B}$ over all possible values of the argument r of sine and cosine functions. The resulting value depends on the natural frequency of the system and turns out to be:

$$r_B = \max\left\{ \frac{1}{\overline{\omega}_0}, \overline{\omega}_0 \right\} = \overline{\omega}_0. \tag{38}$$

For the object of Fig. (4), for which a natural frequency of $\overline{\omega}_0 = 9.56\,\mathrm{s}^{-1}$ can be computed from equation (21) (being R= 7 cm and $g = 9.81\,\mathrm{m/s^2}$), corresponding to a period T_0 of 0.6 s, the rounded value of 10 s^{-1} is assigned to $\overline{\omega}_0$ so that r_B is equal to 10.

Account of the complex eigenvalues of $\boldsymbol{M_C}$ yields for its spectral radius r_{M_C} the expression:

$$r_{M_C} = \frac{\overline{\omega}_0 h^3}{12}\sqrt{h^2\overline{\omega}_0^2 + 1}. \tag{39}$$

Square root of the spectral radius of $\boldsymbol{A}^T\boldsymbol{A}$ provides a bound for the spectral radius of $\boldsymbol{A}$

$$r_A = \sqrt{1+\epsilon}, \tag{40}$$

where

$$\epsilon = \beta + \sqrt{\beta^2 + 2\beta}, \tag{41}$$

with β having the following expression:

$$\beta = \left(\frac{2\sqrt{2}h(\overline{\omega}_0^2 - 1)}{4 + h^2\overline{\omega}_0^2}\right)^2. \tag{42}$$

Elaboration of the bounds associated with the matrix series $\sum_{k=0}^{n-1}\boldsymbol{A}^{(n-k-1)}$ in (37) leads to a geometric series which ultimately results into a bounding term r_{GSA} such that for any vector $\boldsymbol{v}\in\mathbb{R}^2$ the inequality holds:

$$\left\|\sum_{k=0}^{n-1}\boldsymbol{A}^{(n-k-1)}\boldsymbol{v}\right\| \leq r_{GSA}\,\|\boldsymbol{v}\| \tag{43}$$

Upon further bounding based on notable limits, omitted here for brevity, the following inequality finally holds:

$$r_{GSA} = \frac{r_A^n - 1}{r_A - 1} \leq M_{GSA}, \quad \text{where } M_{GSA} = \frac{3t^*}{h}, \tag{44}$$

being $t^* = nh$. Collecting all partial bounds, the finally resulting error bounding expression is $M_n^{(n)} = M_{GSA}r_{M_C}r_B$. This bound has been empirically tested with the linearized half-disk oscillator problem for which a sufficiently accurate reference comparison solution can be constructed from Matlab's [15] in-built sine and cosine functions.

Fig. (5) shows the results of a comparative analysis of three collocation methods and tests the predictivity of the proposed error bounding method, applied to midpoint collocation. The linearized half disk model (with small rotations and no friction) has been integrated for the considered testing model problem, corresponding to $\overline{\omega}_0 = 10\,\mathrm{s}^{-1}$, over the time interval $[0;t^*]$, with t^* being one second. Three collocation methods have been applied, associated with $\alpha_c = 0$, $\alpha_c = 1/2$, and $\alpha_c = 1$ with progressively refined time discretizations n. Initial conditions are $\theta_0 = 0.0$ and $\omega_0 = 1.0\,s^{-1}$.

For the three methods, the error $e_n^{(n)}(t^*)$ computed a-posteriori by comparison with the Matlab trigonometric function solution has been diagrammed in double logarithmic scale format.

In Fig. (5)it can be observed that $e_n^{(n)}(t^*)$ is second order accurate for midpoint collocation and is only first order accurate for collocation at extremal time step points, in line with what already observed concerning Eq. (30) and confirming the proper choice of midpoint collocation in the computation presented in Sect. 4.1.

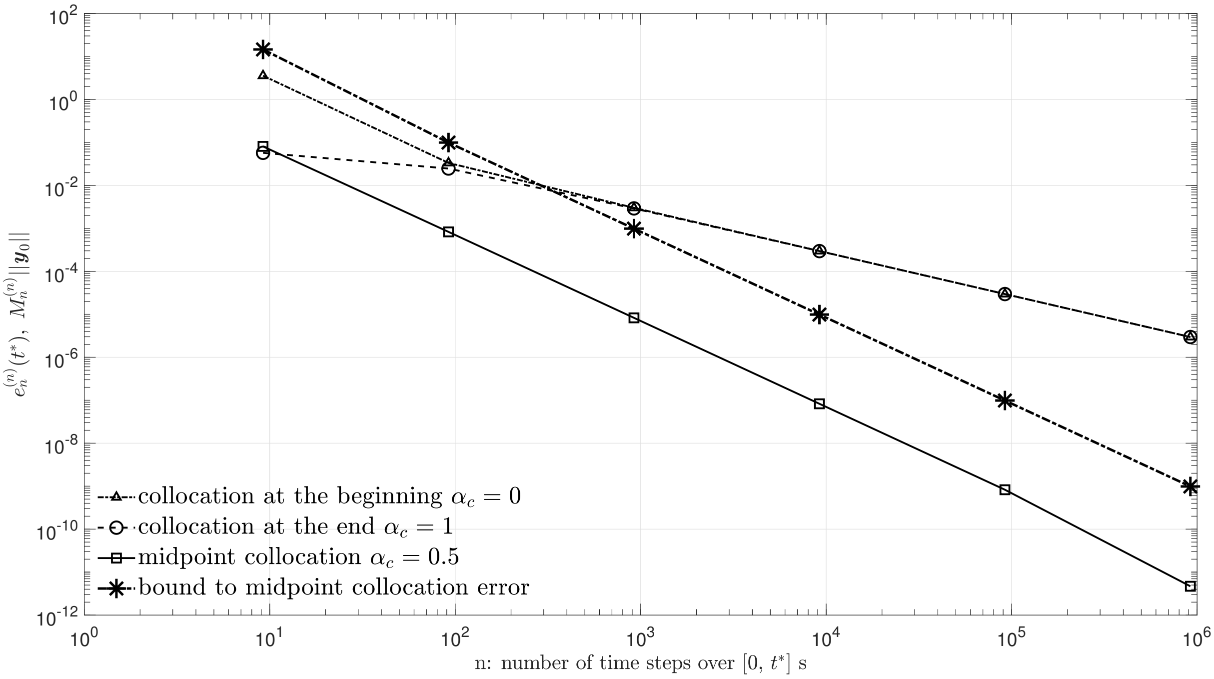

Figure 5: Loglog plot of computed error and error bound

5 CONCLUSIONS

This study has compared different collocation methods for integrating the differential equation governing the dynamics of a rolling half disk model which is being investigated by the authors.

By employing power series expansions, the method of indeterminate coefficients, Leibniz theorem and an analysis of the spectral radii of the matrices involved in the proposed algorithimic procedure, the study could provide an effective methodology for theoretically determining an a-priori bound to computational error for midpoint collocation. The effectiveness of this bound has been succesfully verified by a-posteriori comparison (after computation) with the actual error experimented in numerical results. Investigation for further improving, fine-tuning and theoretically generalizing the bounding methodologies employed in this study certainly deserves consideration. The results obtained seem to deserve attention for their fundamental connection with more general oscillatory problems, also considering that a review of general texts on computational methods could not retrieve explicit expressions for such class of error bounds [11], [12], [13] ,[14]. The comparison carried out in this study among the employed midpoint collocation scheme and other collocation methods has shown, both theoretically and empirically, the optimality of midpoint collocation.

The methodologies which in this opening study have been focused on the simpler condition of small displacements are currently being investigated by the authors also for the more general half disk problem with large rotations and in presence of friction, and for a comparison with methods of the Newmark family [10, 13].

Given the simplicity and generality of the midpoint collocation schemes and of normal form treatment of differential equations, the methodology herein explored appears to be generalizable to more complex geometries and mechanical systems, such as noncircular bowls and vessels with disparate shapes, as well as to assemblages of rigid objects.

REFERENCES

[1] Sungay, B., Erturk, N., Cakti, E., Erdik, M., & Podany, J. (2010). Recent efforts in Istanbul to protect museum collections from damage due to earthquakes. Proceedings for IIC Istanbul Congress 2010. International Institute for Conservation of Historic and Artistic Works.

[2] De Lillo, A. (2020). 19.34/ Quaranta anni dopo/La storia in presa diretta. Fotografie di Antonietta De Lillo, mostra del 23 novembre 2023. Web reference: `https://www.arte.it/calendario-arte/napoli/mostra-19-34-quaranta-anni-dopo-la-storia-in-presa-diretta-\fotografie-di-antonietta-de-lillo-72711`

[3] Sallicandro, E., Serpieri, R., Monaco, M. (2024a). Time-history analysis of sliding-rolling mechanical systems. Proceedings for Gimc Simai Young 2024, Naples, Italy.

[4] Sallicandro, E., Serpieri, R., Monaco, M. (2024b). Euler-Lagrange analysis of freestanding objects subjected to dynamic excitations. Insights from the half-disk model. Proceedings for XXVI AIMETA congress, Naples, Italy.

[5] Levi Civita, T., Amaldi, U. (1923). *Lezioni di meccanica razionale*. Zanichelli Editore Bologna.

[6] Housner, G.W. (1963). The behavior of inverted pendulum structures during earthquakes. *Bulletin of the Seismological Society of America*, 53(2), 403–417.

[7] Coccia, S., Como, M., Di Carlo, F. (2022). The slender rigid block: archetype for the seismic analysis of masonry structures. *Journal of Earthquake Engineering*.

[8] Coulomb, C.A. (1821). *Théorie des machines simples, en ayant égard au frottement de leurs parties et à la roideur des cordages*, Bachelier, Paris.

[9] Monaco, M., Guadagnuolo, M., Gesualdo, A. (2014). The role of friction in the seismic risk mitigation of freestanding art objects. *Natural Hazards*.

[10] Newmark, N. M. (1959). A method of computation for structural dynamics. *Journal of Engineering Mechanics Division, ASCE*.

[11] Bachvalov, N. S. (1980). *Metodi numerici*, Editori Riuniti, Edizioni Mir.

[12] Demidovic, B. et al. (1981). *Esercizi e problemi di analisi matematica*, Editori Riuniti, Edizioni Mir.

[13] Hughes, T.J.R. (2000). *The finite element method: linear static and dynamic- Finite element Analysis*, Dover Publications Inc.

[14] Quarteroni, A. et al. (2017). *Calcolo scientifico, 6° edizione*, Springer.

[15] The MathWorks Inc. (2022). MATLAB version: 9.13.0 (R2022b), Natick, Massachusetts. `https://www.mathworks.com`